A Tensor Artificial Viscosity using a Mimetic Finite Difference Algorithm

J.C. Campbell[†] and M.J. Shashkov[‡]

[†] *T-7 and T-CNLS, Los Alamos National Laboratory, Los Alamos, New Mexico, 87545*
[‡] *T-7, Los Alamos National Laboratory, Los Alamos, New Mexico, 87545*

E-mail: jamesc@lanl.gov

LA-UR-00-4507

We have developed a multi-dimensional tensor artificial viscosity for finite difference shock wave computations. The discrete viscosity tensor is formed by multiplying the gradient of velocity tensor by a scalar term. The scalar term is based on the form of viscosity first presented by Kurapatanko, and also contains a limiter term designed to switch off the viscosity for shock-less compression and rigid-body rotation. Mimetic discretizations are used to derive forms of the momentum and energy equations for a nonorthogonal grid with the viscosity tensor evaluated at the zone edges. The advantage of the tensor viscosity is a reduction in the grid dependence of the solution

1. INTRODUCTION

In this paper we describe the introduction of a tensor artificial viscosity in a Lagrangian hydrodynamics code. The governing equations of a Lagrangian code are the momentum (1) and energy equations (2), which are written

$$\rho \frac{d\mathbf{v}}{dt} = -\nabla P \ , \tag{1}$$

$$\rho \frac{de}{dt} = -P \ \nabla \cdot \mathbf{v} \ , \tag{2}$$

where ρ is density, P is pressure, e is specific internal energy and $\mathbf{v}$ is the velocity vector.

If the hydrodynamics code is intended to solve problems involving shock waves then special methods are required to model the shock wave as, without these, post-shock oscillation will destroy the solution. A standard method is the introduction of an artificial viscosity term.

The pioneering artificial viscosity was developed by Von Neumann and Richtmyer [16] for one dimensional shock wave calculations. Their approach was to modify the momentum and energy equations by adding a dissipative, viscosity like, term to the pressure that would produce a shock wave thickness on the order of to the spacing of the computational mesh. This term could be any function that satisfied the following constraints: the modified conservation equations must possess solutions without discontinuities, the Hugoniot equations must hold when all other dimensions are large compared to the shock thickness, and the dissipative term must be negligible outside of the shock wave. Their viscosity had the form

$$q = -\rho \Delta \mathbf{v} |\Delta \mathbf{v}| \ . \tag{3}$$

This term is quadratic in $\Delta \mathbf{v}$, is positive in compression and negative in expansion. As expansion does not require the viscosity term to give a stable solution, it is common to set $q = 0$ when $\Delta \mathbf{v} > 0$.

When using (3) nonphysical oscillations were still seen behind the shock wave. To remove these oscillations Landshoff [10] added a second term to q that was linear in $\Delta \mathbf{v}$ and so vanished less rapidly behind a shock wave

$$q = c_L \rho c_s |\Delta \mathbf{v}| + c_Q \rho (\Delta \mathbf{v})^2 \tag{4}$$

here c_s is the local sound speed and c_L and c_Q are non-dimensional constants, c_L multiplying the linear term and c_Q the quadratic. This basic form of viscosity has become widely used.

Another form of the viscosity term was described by Wilkins [17] who attributed it to Kurapatenko [9].

$$q_{Kur} = \rho \left\{ c_2 \frac{(\gamma+1)}{4} |\Delta \mathbf{v}| + \sqrt{c_2^2 \left(\frac{\gamma+1}{4} \right)^2 (\Delta \mathbf{v})^2 + c_1^2 c_s^2} \right\} |\Delta \mathbf{v}| \tag{5}$$

where c_1 and c_2 are non-dimensional constants, and γ is the ratio of specific heats. This expression will be referred to as the Kurapatenko form of viscosity. The expression was derived from the pressure jump across a shock in an ideal gas. With $c_1 = c_2 = 1$, ρ and c_s the density and sound speed ahead of the shock and $\Delta \mathbf{v}$ the velocity jump across the shock, the equation gives the pressure jump across it. Equation (5) reduces to the linear term of the basic shock viscosity as $\Delta \mathbf{v} \to 0$ and the quadratic term as $c_s \to 0$ or when $\Delta \mathbf{v}$ becomes large.

In a one dimensional calculation $\Delta \mathbf{v}$ is clearly defined. The simplest extension to n dimensions is to treat the viscosity as a pressure term and set $\Delta \mathbf{v} \approx \sqrt[n]{V} (\nabla \cdot \mathbf{v})$, where V is the zone volume. A more accurate extension is to take the velocity jump across the zone in the direction of the shock, but reliably calculating the shock direction is difficult and can introduce problems of its own. For a review of viscosity formulations see Benson [1].

Recently Caramana et al. [5] specified five properties that an artificial viscosity should possess, these are

1. Dissipativity: The artificial viscosity must only act to decrease kinetic energy.
2. Galilean invariance: The viscosity should vanish smoothly as the velocity field becomes constant.

3. Self-similar motion invariance: The viscosity should vanish for uniform contraction and rigid rotation.

4. Wave-front invariance: The viscosity should have no effect along a wave front of constant phase, on a grid aligned with the shock wave.

5. Viscous force continuity: The viscous force should go to zero continuously as compression vanishes and remain zero for expansion.

In the same paper they present an edge viscosity for Lagrangian codes which satisfies these conditions. A common test problem for shock wave codes is the Noh problem [12], where a volume of gas is given an initial inward radial velocity and a strong shock wave is generated at the point of convergence. Results presented for this problem in [5] deal with Lagrangian grids aligned with the flow. However with an initially square grid, jets are formed along the axes which results in a highly deformed mesh, Fig. 3. Our opinion is that the reason for this is that the edge viscosity [5] does not model physical viscosity, and therefore does not have a well defined continuum limit. As a consequence it has a very random dependence on the grid.

The aim of the work described here was to develop a viscosity which retains the useful features of the edge viscosity, but is based on an approximation to a quantity which may be related to physical viscosity, and has a tensor nature. As an artificial viscosity stress tensor does not have to be symmetric, we consider a viscosity of the form

$$\mathbf{Q} = \mu \mathbf{G}^{\mathrm{T}} \tag{6}$$

where $\mathbf{G} = \nabla \mathbf{v}$ and μ is a scalar coefficient. We construct the discrete equations so that the viscosity tensor is held on zone edges as a tangential projection to the edge. This is natural for a staggered discretization where velocity components are given at grid nodes. As we show by numerical experiment, using a tensor viscosity with this basic form reduces dependence of the numerical solution on the grid.

The next section gives a brief description of Caramana's edge viscosity, and shows results from the Noh problem an initially square grid. Section 3 discusses the general form of the viscosity, and what constraints must be placed on the form of the viscosity coefficient in order to satisfy the five properties. In section 4 expressions for the divergence of a tensor and gradient of a vector in a general curvilinear coordinate system are derived. These expressions are then used in section 5 to develop the discrete operators required to implement the tensor viscosity. Then section 6 describes the actual form of viscosity coefficient used, and the implementation of the viscosity in the test code. In section 7 results from three test problems are shown, comparing the edge viscosity to the new tensor viscosity. Finally the conclusions are given in section 8.

2. EDGE VISCOSITY

In this section we briefly describe the edge viscosity developed by Caramana et al. [5], and introduce some notations which we will use later.

We assume a spatially staggered grid where pressure, density and energy are given in the zones and velocity at the points. Each zone is subdivided by the

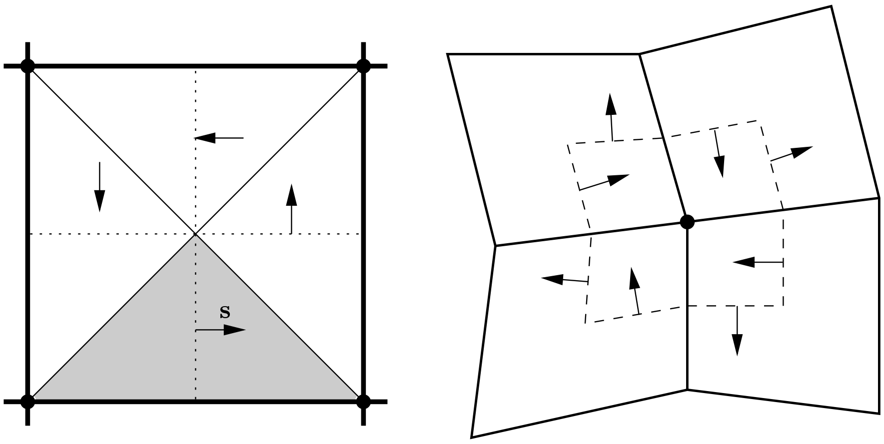

a b

FIG. 1. (a) A quadrilateral zone. The solid lines show the boundaries of the triangular subzones, one subzone is shaded. The dotted lines show the median mesh. The vectors normal to the median mesh, $\mathbf{s}$, are defined as positive in the direction shown. (b) Integration path around median mesh for central node.

median mesh which connects the center of the zone to the middle of each edge, Fig. 1a. The median mesh defines the control volume used to calculate the nodal forces through the momentum equation, Fig. 1b. The vector $\mathbf{s}$ is the normal to the median mesh, the magnitude of the vector is equal to the length of the associated section of the median mesh.

For the edge viscosity each zone is split into four triangular subzones, each subzone defined by the two nodes on an edge and the zone center Fig. 1a. The viscosity is taken to be constant inside each of these subzones. The nodal acceleration can then be calculated using the compatible finite difference method of integrating around the median mesh surrounding each node [3]. The median mesh around a point is an eight-sided figure and the viscosity is constant along each side.

Edge k connects the two points b and c, Fig. 2. For the subzone in zone z associated with edge k the viscosity force is

$$\mathbf{f}_k = \begin{cases} (1-\psi_k) q_{Kur,k} (\widehat{\Delta\mathbf{v}_k} \cdot \mathbf{s}_c^z) \widehat{\Delta\mathbf{v}_k} & \text{if } (\Delta\mathbf{v}_k \cdot \mathbf{s}_c^z) < 0 \\ 0 & \text{if } (\Delta\mathbf{v}_k \cdot \mathbf{s}_c^z) \geq 0 \ . \end{cases} \tag{7}$$

$\mathbf{f}_k$ contributes to the total force at points b and c. The velocity difference for the edge is $\Delta\mathbf{v}_k = \mathbf{v}_b - \mathbf{v}_c$, and $\widehat{\Delta\mathbf{v}_k}$ is the unit vector in the direction of this velocity difference. For the edge the density and sound speed are

$$\rho_k = \frac{2\rho_b\rho_c}{\rho_b + \rho_c} \quad , \quad c_{s,k} = \min(c_{s,b}, c_{s,c}) \ . \tag{8}$$

The density and sound speed at a node is the volume weighted average of the surrounding zones. The final term to define is ψ_k which is a limiter function that acts to switch off the viscosity for self-similar motion and along wave fronts of

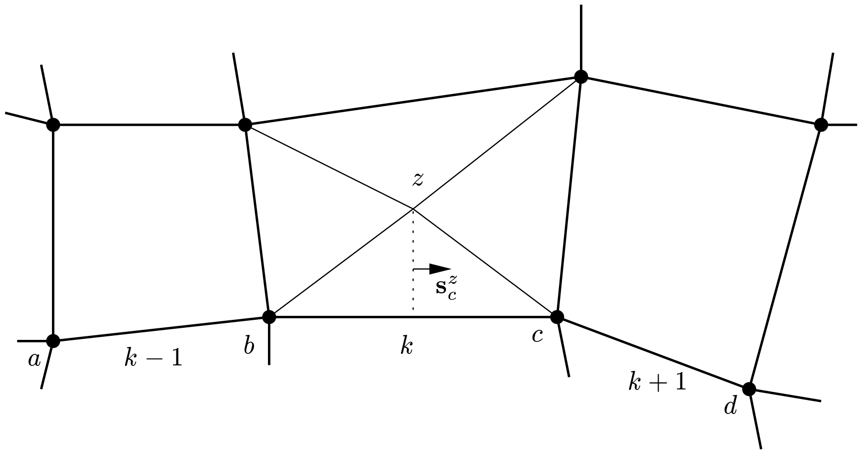

FIG. 2. A section of a logical mesh showing edge k and its neighbor edges.

constant phase. The function is defined as

$$\psi_k = \max[0, \min(0.5(r_{l,k} + r_{r,k}) \, , \, 2r_{l,k} \, , \, 2r_{r,k} \, , \, 1)] \, , \tag{9}$$

$$r_{r,k} = \frac{\Delta\mathbf{v}_{k+1} \cdot \widehat{\Delta\mathbf{v}}_k}{\Delta\mathbf{x}_{k+1} \cdot \widehat{\Delta\mathbf{x}}_k} \Bigg/ \frac{|\Delta\mathbf{v}_k|}{|\Delta\mathbf{x}_k|} \quad , \quad r_{l,k} = \frac{\Delta\mathbf{v}_{k-1} \cdot \widehat{\Delta\mathbf{v}}_k}{\Delta\mathbf{x}_{k-1} \cdot \widehat{\Delta\mathbf{x}}_k} \Bigg/ \frac{|\Delta\mathbf{v}_k|}{|\Delta\mathbf{x}_k|} \quad . \tag{10}$$

Fig. 2 shows how the left and right edges are defined on a logical grid. On an unstructured grid the neighbor edges are found by checking all edges that meet at an end point, and selecting the edge which forms the largest angle with the center edge.

The term ψ is a multi-dimensional form of a one dimensional TVD advection limiter. The limiter is used to switch off the viscosity when the second derivative of the velocity field is zero and has the advantage that the second derivative does not have to be actually calculated. The limiter term ensures that the viscosity satisfies the conditions of self-similar motion invariance and wave front invariance.

The edge viscosity satisfies the condition of Galilean invariance as the force is an explicit function of $\Delta\mathbf{v}_k$. Viscous force continuity is satisfied because the on/off switch $(\Delta\mathbf{v}_k \cdot \mathbf{s}_c^z)$ also appears in the force expression.

The contribution from the viscous force in a subzone to the zone internal energy is $-\mathbf{f}_k \cdot \Delta\mathbf{v}_k$, $\mathbf{f}_k$ is proportional to $|\Delta\mathbf{v}_k|$, and is only non-zero if $\Delta\mathbf{v}_k$ is negative. So Dissipativity is satisfied because the change in internal energy is proportional to $(\Delta\mathbf{v}_k)^2$, and so must be positive.

Fig. 3 shows results for the cylindrical Noh problem. The cylindrical Noh problem assumes 2D plane strain. A volume of perfect gas is given an initial unit inward radial velocity. A circular shock wave is generated from the center of convergence and propagates away from the center. At time 0.6 the analytic solution gives the shock wave a radius of 0.2. This can be seen for the polar mesh. The jets that have formed along the axes with the initially Cartesian mesh and the consequent mesh distortion are clear in the figure. Although the result shown used symmetry

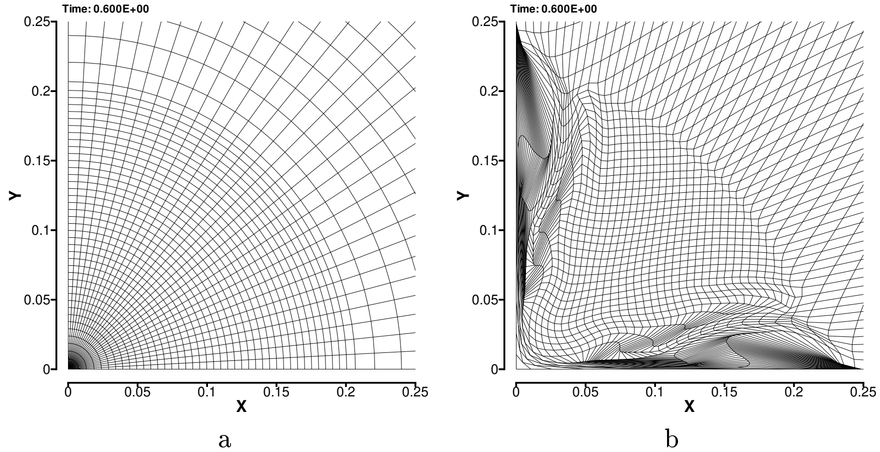

FIG. 3. Cylindrical Noh problem results for edge viscosity on a polar mesh (a) and a Cartesian mesh (b).

planes along the x and y axes the jets are not a boundary condition effect. The same results are seen if symmetry planes are not used, and the whole volume is covered by the grid.

The viscosity force in equation (7) can be written as the product of a tensor with vector **s**, [5]. However this tensor is not a real tensor in the sense that even for smooth parameters **Q** in one zone can change dramatically. As a consequence this viscosity does not have a well defined continuum limit, which we believe causes the problems with the numerical solution shown in Fig. 3b.

3. CONTINUOUS FORM OF TENSOR ARTIFICIAL VISCOSITY

For our new tensor viscosity we start by assuming a form similar to physical viscosity. It is not necessary for an artificial viscosity to be symmetric; so we use the gradient of velocity tensor **G** rather than the symmetric rate of deformation tensor used for physical viscosity. We define the viscosity tensor, **Q**, as

$$\mathbf{Q} = \mu \mathbf{G}^{\mathrm{T}} \ . \tag{11}$$

where μ is a scalar coefficient. For this viscosity tensor the momentum and energy equations, considering only the viscosity terms, become

$$\rho \frac{d\mathbf{v}}{dt} = \nabla \cdot \mathbf{Q}^{\mathrm{T}} = \nabla \cdot (\mu \mathbf{G}) \tag{12}$$

$$\rho \frac{de}{dt} = \mathbf{Q} \cdot\cdot \mathbf{G} = \mu \mathbf{G} : \mathbf{G} \ . \tag{13}$$

where $\mathbf{Q}\cdot\cdot\mathbf{G} = Q_{ij}G_{ji}$, and $\mathbf{G} : \mathbf{G} = G_{ij}G_{ij}$ using the usual summation convention. Using this form of **Q** is conservative.

A nonsymmetric viscosity gives a useful property, there is no mode conversion [11]. This means that for a shear flow in which all velocities are parallel, the viscous force will only act in the velocity direction. With a symmetric tensor viscosity the force would have a component perpendicular to the velocity direction.

In order to ensure dissipativity we need to make sure that the viscosity can only decrease the kinetic energy. So in the energy equation we need to ensure that the $\mathbf{Q}\cdot\cdot\mathbf{G}$ is always positive. With the form of $\mathbf{Q}$ in (11) this is easily satisfied by ensuring $\mu \geq 0$.

Self-similar motion invariance requires that $\mu = 0$ for this case, this can be achieved by including a limiter function similar to that used for the edge viscosity. Galilean invariance is satisfied because as the velocity field becomes constant, all terms in $\mathbf{G}$ become zero.

Viscous force continuity requires some switch to ensure that $\mu = 0$ for expansion. For the tensor viscosity a clear choice for defining compression and expansion is the divergence of velocity. However this switch will only partly satisfy the condition, the viscosity force should also go to zero smoothly. The edge viscosity contains the term that is used to detect compression and expansion, as this term multiples all other terms in the force equation it ensures that the force does go to zero smoothly. For the tensor viscosity there is no equivalent term, so compression and expansion must be detected by a term not present in the viscosity, but this does not ensure that the viscosity will go to zero smoothly as compression vanishes. In order to satisfy viscous force continuity a non-dimensional term would have to be added to the viscosity. For the results presented here this has not been done and so the viscosity does not fully satisfy this condition.

The final property, wave-front invariance, is satisfied because of the functional form of viscosity, so the limiter function is only required to ensure self-similar motion invariance. To check for wave front invariance we will take the case of radial flow, which was used in [5] to show wave front invariance for the edge viscosity. For 2D cylindrical coordinates (r, θ) the velocity gradient tensor is

$$\mathbf{Q} = \mu \begin{bmatrix} \dfrac{\partial v_r}{\partial r} & \dfrac{\partial v_\theta}{\partial r} \\ \\ \dfrac{1}{r}\dfrac{\partial v_r}{\partial \theta} - \dfrac{v_\theta}{r} & \dfrac{1}{r}\dfrac{\partial v_\theta}{\partial \theta} + \dfrac{v_r}{r} \end{bmatrix} \tag{14}$$

and the momentum equation is

$$\begin{aligned} \rho a_r &= \frac{\partial Q_{rr}}{\partial r} + \frac{1}{r}\frac{\partial Q_{\theta r}}{\partial \theta} + \frac{1}{r}(Q_{rr} - Q_{\theta\theta}) \\ \rho a_\theta &= \frac{\partial Q_{r\theta}}{\partial r} + \frac{1}{r}\frac{\partial Q_{\theta\theta}}{\partial \theta} + \frac{1}{r}(Q_{r\theta} - Q_{\theta r}) \ . \end{aligned} \tag{15}$$

For radial flow $v_\theta = 0$ and $\frac{\partial v_r}{\partial \theta} = 0$ so for our viscosity the momentum equation becomes

$$\begin{aligned} \rho a_r &= \frac{\partial}{\partial r}\left(\mu \frac{\partial v_r}{\partial r}\right) + \frac{\mu}{r}\frac{\partial v_r}{\partial r} \\ \rho a_\theta &= 0 \ . \end{aligned} \tag{16}$$

As the viscosity only produces accelerations in the radial direction, it satisfies the condition of wave-front invariance.

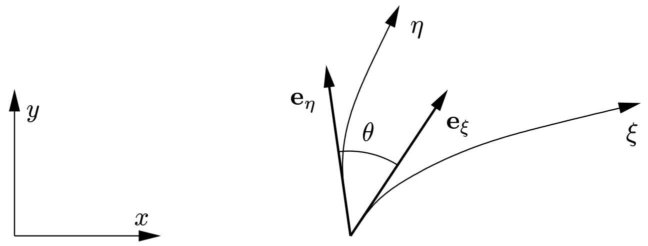

FIG. 4. Base vectors of general coordinate system (ξ, η). θ is the angle between the vectors tangential to the coordinate system.

4. GRADIENT OF A VECTOR AND DIVERGENCE OF A TENSOR IN A GENERAL COORDINATE SYSTEM

To implement the tensor viscosity we need expressions for the divergence of a tensor and the gradient of a vector. To introduce limiters and retain good properties of the edge viscosity, it will be useful for us to write these operators using a general curvilinear coordinate system. This will allow the discrete viscosity to be held tangential to the zone edges. In this section we derive continuous expressions for the divergence and gradient for a general coordinate system. We consider the continuous case as it acts as a guide when we come to derive the discrete expressions.

We use two coordinate systems, for simplicity we consider only the 2D case. The first is the standard rectangular Cartesian coordinate system, (x, y). The second is a general curvilinear system, (ξ, η), with base vectors $\mathbf{e}_\xi$ and $\mathbf{e}_\eta$ tangential to the coordinate lines. These are shown in Fig. 4. The Cartesian components of the basis vectors are

$$\mathbf{e}_\xi = \begin{pmatrix} \dfrac{\partial x}{\partial \xi} \\ \\ \dfrac{\partial y}{\partial \xi} \end{pmatrix} \quad , \quad \mathbf{e}_\eta = \begin{pmatrix} \dfrac{\partial x}{\partial \eta} \\ \\ \dfrac{\partial y}{\partial \eta} \end{pmatrix} . \tag{17}$$

It is also useful to know the metric tensor relative to the general coordinate system. The components of the metric tensor are

$$g_{\xi\xi} = \mathbf{e}_\xi \cdot \mathbf{e}_\xi \quad , \quad g_{\eta\eta} = \mathbf{e}_\eta \cdot \mathbf{e}_\eta \quad , \quad g_{\xi\eta} = g_{\eta\xi} = \mathbf{e}_\eta \cdot \mathbf{e}_\xi \quad . \tag{18}$$

From these the determinant of the metric tensor can be found, which we write as $|g|$.

The gradient of velocity tensor, $\mathbf{G}$, is defined as

$$\mathbf{G} = \nabla \mathbf{v} \tag{19}$$

or in tensor index notation

$$G_{ij} = \frac{\partial v_i}{\partial x_j} \tag{20}$$

where $x_1 = x$, $x_2 = y$ and $\mathbf{v} = [v_1,\ v_2] = [v_x,\ v_y]$.

In the general coordinate system a tensor can be represented by two vectors which are projections to two basis vectors. Each vector is the dot product of the tensor with a unit base vector.

$$\mathbf{G}^{\xi} = \mathbf{G} \cdot \hat{\mathbf{e}}_{\xi} \;\text{ and }\; \mathbf{G}^{\eta} = \mathbf{G} \cdot \hat{\mathbf{e}}_{\eta} \tag{21}$$

where the hat signifies a unit vector. Then Cartesian components of these vectors can be rewritten in terms of the derivatives of vector $\mathbf{v}$ with respect to ξ and η

$$\mathbf{G}^{\xi} = \frac{1}{\sqrt{g_{\xi\xi}}} \begin{pmatrix} \dfrac{\partial v_x}{\partial \xi} \\ \\ \dfrac{\partial v_y}{\partial \xi} \end{pmatrix} = \begin{pmatrix} \mathbf{G}^{\xi x} \\ \\ \mathbf{G}^{\xi y} \end{pmatrix} \;,\; \mathbf{G}^{\eta} = \frac{1}{\sqrt{g_{\eta\eta}}} \begin{pmatrix} \dfrac{\partial v_x}{\partial \eta} \\ \\ \dfrac{\partial v_y}{\partial \eta} \end{pmatrix} = \begin{pmatrix} \mathbf{G}^{\eta x} \\ \\ \mathbf{G}^{\eta y} \end{pmatrix} . \tag{22}$$

For future considerations in the discrete case, it is useful to derive an expression for the divergence in terms of tangential projections of a tensor using the integral identity

$$\int_V \nabla \mathbf{v} : \mathbf{T} dV = \oint_{\partial V} \mathbf{v} \cdot (\mathbf{T} \cdot \mathbf{n}) dS - \int_V \mathbf{v} \cdot (\nabla \cdot \mathbf{T}) dV \tag{23}$$

where $\mathbf{T}$ is any second order tensor.

To use the identity an expression for the scalar product in terms of the tangential projections is required. The scalar product is defined in terms of the Cartesian components of the two tensors, so we start by defining the Cartesian components of $\mathbf{G}$ in terms of $\mathbf{G}^{\xi}$ and $\mathbf{G}^{\eta}$. These formulae are valid for any tensor, and are found by solving the set of equations represented by equation (21)

$$\begin{aligned} G_{xx} &= \frac{\sqrt{g_{\xi\xi}}}{\sqrt{|g|}} \frac{\partial y}{\partial \eta} \mathbf{G}^{\xi x} - \frac{\sqrt{g_{\eta\eta}}}{\sqrt{|g|}} \frac{\partial y}{\partial \xi} \mathbf{G}^{\eta x} \\ G_{xy} &= \frac{\sqrt{g_{\eta\eta}}}{\sqrt{|g|}} \frac{\partial x}{\partial \xi} \mathbf{G}^{\eta x} - \frac{\sqrt{g_{\xi\xi}}}{\sqrt{|g|}} \frac{\partial x}{\partial \eta} \mathbf{G}^{\xi x} \\ G_{yx} &= \frac{\sqrt{g_{\xi\xi}}}{\sqrt{|g|}} \frac{\partial y}{\partial \eta} \mathbf{G}^{\xi y} - \frac{\sqrt{g_{\eta\eta}}}{\sqrt{|g|}} \frac{\partial y}{\partial \xi} \mathbf{G}^{\eta y} \\ G_{yy} &= \frac{\sqrt{g_{\eta\eta}}}{\sqrt{|g|}} \frac{\partial x}{\partial \xi} \mathbf{G}^{\eta y} - \frac{\sqrt{g_{\xi\xi}}}{\sqrt{|g|}} \frac{\partial x}{\partial \eta} \mathbf{G}^{\xi y} \;. \end{aligned} \tag{24}$$

Now it is possible to write down the scalar product and collect terms to get

$$\begin{aligned} \mathbf{G} : \mathbf{T} \;=\; & \mathbf{G}^{\xi} \cdot \left[\mathbf{T}^{\xi} \frac{g_{\xi\xi} g_{\eta\eta}}{|g|} - \mathbf{T}^{\eta} \frac{g_{\xi\eta}}{|g|} \sqrt{g_{\xi\xi}} \sqrt{g_{\eta\eta}} \right] + \\ & \mathbf{G}^{\eta} \cdot \left[\mathbf{T}^{\eta} \frac{g_{\xi\xi} g_{\eta\eta}}{|g|} - \mathbf{T}^{\xi} \frac{g_{\xi\eta}}{|g|} \sqrt{g_{\xi\xi}} \sqrt{g_{\eta\eta}} \right] . \end{aligned} \tag{25}$$

Rearranging and noting that

$$\frac{g_{\xi\xi} g_{\eta\eta}}{|g|} = \frac{1}{\sin^2 \theta} \;,\; \frac{g_{\xi\eta}}{\sqrt{g_{\xi\xi}} \sqrt{g_{\eta\eta}}} = \cos\theta \tag{26}$$

allows the scalar product to be written only in terms of the tangential projections and the angle θ between $\mathbf{e}_\xi$ and $\mathbf{e}_\eta$, Fig 4.

$$\mathbf{G}:\mathbf{T} = \frac{1}{\sin^2\theta}\Big[\mathbf{G}^\xi\cdot\mathbf{T}^\xi + \mathbf{G}^\eta\cdot\mathbf{T}^\eta - \cos\theta(\mathbf{G}^\xi\cdot\mathbf{T}^\eta + \mathbf{G}^\eta\cdot\mathbf{T}^\xi)\Big]. \tag{27}$$

Comparing (27) to the expression for the vector dot product in [7] shows that the two expressions are equivalent except that the ξ and η terms are vectors in our case.

In deriving an expression for the divergence using the identity in (23) we assume, for simplicity, that the surface integral is zero. Then use equation (24) for $\nabla\mathbf{v}:\mathbf{T}$ and replace the $\mathbf{G}^\xi$ and $\mathbf{G}^\eta$ terms with the derivatives of vector $\mathbf{v}$ using (22). This gives

$$\begin{aligned}\iint \nabla\mathbf{v}:\mathbf{T}\sqrt{|g|}d\xi d\eta = \iint\Bigg(& \frac{\partial\mathbf{v}}{\partial\xi}\cdot\left[\frac{\mathbf{T}^\xi - \cos\theta\mathbf{T}^\eta}{\sqrt{g_{\xi\xi}}\sin^2\theta}\right] + \\ & \frac{\partial\mathbf{v}}{\partial\eta}\cdot\left[\frac{\mathbf{T}^\eta - \cos\theta\mathbf{T}^\xi}{\sqrt{g_{\eta\eta}}\sin^2\theta}\right]\Bigg)\sqrt{|g|}d\xi d\eta\,.\end{aligned} \tag{28}$$

Integrating this expression by parts gives two terms that are equivalent to the RHS of equation (23). Ignoring the terms representing the surface integral leaves

$$\begin{aligned}\iint \mathbf{v}\cdot(\nabla\cdot\mathbf{T})\sqrt{|g|}d\xi d\eta = \iint\Bigg(& \mathbf{v}\cdot\frac{\partial}{\partial\xi}\left[\sqrt{|g|}\frac{\mathbf{T}^\xi - \cos\theta\mathbf{T}^\eta}{\sqrt{g_{\xi\xi}}\sin^2\theta}\right] + \\ & \mathbf{v}\cdot\frac{\partial}{\partial\eta}\left[\sqrt{|g|}\frac{\mathbf{T}^\eta - \cos\theta\mathbf{T}^\xi}{\sqrt{g_{\eta\eta}}\sin^2\theta}\right]\Bigg)d\xi d\eta\,.\end{aligned} \tag{29}$$

Now we can write the expression for the divergence

$$\begin{aligned}\nabla\cdot\mathbf{T} = \frac{1}{\sqrt{|g|}}\Bigg\{ & \frac{\partial}{\partial\xi}\left[\sqrt{|g|}\frac{\mathbf{T}^\xi - \cos\theta\mathbf{T}^\eta}{\sqrt{g_{\xi\xi}}\sin^2\theta}\right] + \\ & \frac{\partial}{\partial\eta}\left[\sqrt{|g|}\frac{\mathbf{T}^\eta - \cos\theta\mathbf{T}^\xi}{\sqrt{g_{\eta\eta}}\sin^2\theta}\right]\Bigg\}.\end{aligned} \tag{30}$$

This can also be derived directly from the expression for the divergence in terms of T_{xx}, T_{yy} and T_{xy}. However from a methodological point of view it is useful to derive it using the integral identity.

5. DISCRETE OPERATORS

This section describes the derivation of discrete forms of the gradient of a vector and divergence of a tensor on a grid. The derivation shown uses tangential projections to zone edges, and is an extension of the mimetic finite difference method [7,8,15] to second order tensors. In the mimetic finite difference method a discrete approximation for a differential operator, such as divergence or gradient, is

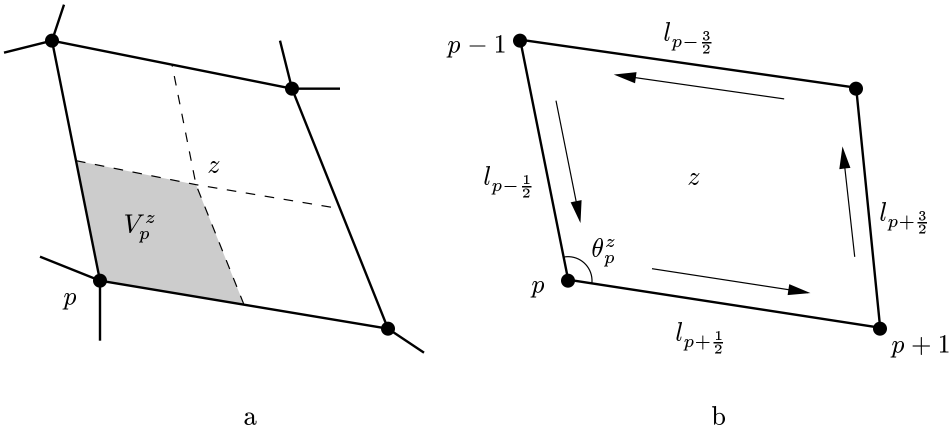

FIG. 5. (a) Fragment of a staggered grid, including zone z and point p. The solid lines show the grid and the dashed lines show the median mesh. The shaded area shows a subzonal Lagrangian volume. (b) We choose notation relative to the currently selected point p, which is a vertex of zone z. The arrows next to each edge show the positive direction of $\hat{\mathbf{e}}$.

chosen. This initial or prime operator then supports the derivation of other discrete operators.

5.1. Grid

We construct the discrete functions on a spatially staggered grid. Fig. 5a shows a section of the staggered grid. The median mesh is constructed by connecting the zone centers with the mid-side points. A core assumption for a Lagrangian method is that each zone of the grid represents a discrete volume element that may deform, but may not gain or lose mass. If the coordinate of the zone center is calculated in a Lagrangian manner then the same assumption can be made for the median mesh. This leads to the definition of a Lagrangian subzonal corner volume, shown in Fig. 5a as the shaded area, which has constant mass. We denote the corner volume as V_p^z, where the indices denote the zone and point with which it is associated. We define $V_p^z = V_z^p$ and follow the convention of always summing with respect to the lower index. The corner volume can then be used to define both a zone volume and a point volume.

$$V_z = \sum_{p \in S(z)} V_p^z \ , \ V_p = \sum_{z \in S(p)} V_z^p, \tag{31}$$

where the sums are over the stencil associated with the zone or point. The stencil for a zone is each point that is a vertex of the zone. For a point the stencil is every adjacent zone. As the mass of a subzone is constant a density is easily defined for the volume. The same super and subscript notation is used for any value that is associated with both a point and a zone.

Fig. 5b shows the notation used for the discrete operators. The notation is all relative to point p, which is a vertex of zone z. $\hat{\mathbf{e}}_{p+\frac{1}{2}}$ is the unit vector along edge $p+\frac{1}{2}$, which connects points p and $p+1$. The arrows shown define the positive direction of $\hat{\mathbf{e}}$. $l_{p+\frac{1}{2}}$ is the length of the edge. θ_p^z is the angle between the two edges of zone z that meet at point p.

5.2. The prime operator

We want expressions for the following two operators: **GRAD**, the discrete form of the vector gradient, and **DIV**, the discrete form of the tensor divergence. For tangential projections to the zone edges **GRAD** is easily defined and so is chosen as the prime operator.

For a given direction l, given by unit vector $\mathbf{l}$, the directional derivative of vector field $\mathbf{v}$ is:

$$\frac{\partial \mathbf{v}}{\partial l} = \mathbf{l} \cdot \nabla \mathbf{v} \ . \tag{32}$$

This leads to the definition of the projections of tensor $\mathbf{G} = \mathbf{GRAD}\ \mathbf{v}$ as

$$\mathbf{G}^e_{p+\frac{1}{2}} = \mathbf{G}_{p+\frac{1}{2}} \cdot \hat{\mathbf{e}}_{p+\frac{1}{2}} = \frac{\mathbf{v}_{p+1} - \mathbf{v}_p}{l_{p+\frac{1}{2}}}. \tag{33}$$

The agreement between equations (33) and (22) is clear when we recall the identities

$$dl_\xi = \sqrt{g_{\xi\xi}}d\xi \ \ , \ \ dl_\eta = \sqrt{g_{\eta\eta}}d\eta \tag{34}$$

where dl_ξ and dl_η are the elements of arcs of coordinate curves.

5.3. The derived operator

We now use the prime operator to derive the discrete divergence, **DIV**, which is the negative adjoint of **GRAD**.

The first step is to get a discrete form of equation (27), the tensor scalar product. We approximate the continuous equation by

$$\begin{aligned}(\mathbf{G}, \mathbf{T})_z = \sum_{p \in S(z)} \frac{W^z_p}{\sin^2 \theta^z_p} \ \Big\{ & \mathbf{G}^e_{p-\frac{1}{2}} \cdot \mathbf{T}^e_{p-\frac{1}{2}} + \mathbf{G}^e_{p+\frac{1}{2}} \cdot \mathbf{T}^e_{p+\frac{1}{2}} \\ & + \cos\theta^z_p \left[\mathbf{G}^e_{p-\frac{1}{2}} \cdot \mathbf{T}^e_{p+\frac{1}{2}} + \mathbf{G}^e_{p+\frac{1}{2}} \cdot \mathbf{T}^e_{p-\frac{1}{2}} \right] \Big\}\end{aligned} \tag{35}$$

which gives the scalar product evaluated in zone z. In this expression the sign of the cosine has changed, this is due to the sign convention adopted. W^z_p are some weights that satisfy the conditions

$$W^z_p \geq 0 \ \ , \ \ \sum_{p \in S(z)} W^z_p = 1. \tag{36}$$

We define W^z_p as one half the area of the triangle in zone z which contains the angle at point p, divided by volume of the zone. For a non-quadrilateral zone this must then be normalized to ensure that the second condition is satisfied. This choice of weights gives a first order approximation of the operator [15].

To derive **DIV** from (35) and (33) we use the discrete form of the integral identity (23) and assume for simplicity that the surface integral is zero. This gives us

$$\sum_z (\mathbf{G}, \mathbf{T})_z V_z = -\sum_p (\mathbf{v}, \mathbf{DIV}\ \mathbf{T})_p V_p. \tag{37}$$

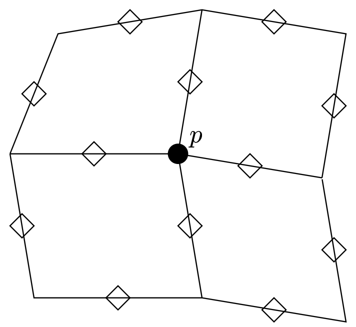

FIG. 6. Stencil for operator $(\mathbf{DIV\ T})_p$ on a logically rectangular grid.

Substitute (35) into (37), and substitute for $\mathbf{G}^e$ using (33). This gives an expression which contains the velocity vector at three points: $\mathbf{v}_{p+1}$, $\mathbf{v}_p$ and $\mathbf{v}_{p-1}$. Then rewriting the expression to collect all the $\mathbf{v}$ terms at point p gives

$$
\begin{aligned}
-\sum_p (\mathbf{v}, \mathbf{DIV\ T})_p V_p \;=\; & \sum_z \sum_{p \in S(z)} \mathbf{v}_p \cdot \Bigg(\\
& \frac{W_p^z}{\sin^2 \theta_p^z} \left\{ \frac{\mathbf{T}^e_{p-\frac{1}{2}}}{l_{p-\frac{1}{2}}} - \frac{\mathbf{T}^e_{p+\frac{1}{2}}}{l_{p+\frac{1}{2}}} + \cos\theta_p^z \left[\frac{\mathbf{T}^e_{p+\frac{1}{2}}}{l_{p-\frac{1}{2}}} - \frac{\mathbf{T}^e_{p-\frac{1}{2}}}{l_{p+\frac{1}{2}}} \right] \right\} \\
& + \frac{W_{p-1}^z}{\sin^2 \theta_{p-1}^z} \left\{ \frac{\mathbf{T}^e_{p-\frac{1}{2}}}{l_{p-\frac{1}{2}}} + \cos\theta_{p-1}^z \frac{\mathbf{T}^e_{p-\frac{3}{2}}}{l_{p-\frac{1}{2}}} \right\} \\
& - \frac{W_{p+1}^z}{\sin^2 \theta_{p+1}^z} \left\{ \frac{\mathbf{T}^e_{p+\frac{1}{2}}}{l_{p+\frac{1}{2}}} + \cos\theta_{p+1}^z \frac{\mathbf{T}^e_{p+\frac{3}{2}}}{l_{p+\frac{1}{2}}} \right\} \Bigg) V_z.
\end{aligned}
\tag{38}
$$

Now an expression for $\mathbf{DIV\ T}$ at a point can be found

$$
\begin{aligned}
(\mathbf{DIV\ T})_p \;=\; & \frac{1}{V_p} \sum_{z \in S(p)} V_z \Bigg[\frac{1}{l_{p+\frac{1}{2}}} \left\{ \frac{W_z^{p+1}}{\sin^2 \theta_z^{p+1}} \left(\mathbf{T}^e_{p+\frac{1}{2}} + \cos\theta_z^{p+1} \mathbf{T}^e_{p+\frac{3}{2}} \right) \right\} \\
& + \frac{1}{l_{p+\frac{1}{2}}} \left\{ \frac{W_z^p}{\sin^2 \theta_z^p} \left(\mathbf{T}^e_{p+\frac{1}{2}} + \cos\theta_z^p \mathbf{T}^e_{p-\frac{1}{2}} \right) \right\} \\
& - \frac{1}{l_{p-\frac{1}{2}}} \left\{ \frac{W_z^p}{\sin^2 \theta_z^p} \left(\mathbf{T}^e_{p-\frac{1}{2}} + \cos\theta_z^p \mathbf{T}^e_{p+\frac{1}{2}} \right) \right\} \\
& - \frac{1}{l_{p-\frac{1}{2}}} \left\{ \frac{W_z^{p-1}}{\sin^2 \theta_z^{p-1}} \left(\mathbf{T}^e_{p-\frac{1}{2}} + \cos\theta_z^{p-1} \mathbf{T}^e_{p-\frac{3}{2}} \right) \right\} \Bigg].
\end{aligned}
\tag{39}
$$

Fig. 6 shows the stencil for operator $(\mathbf{DIV\ T})_p$. In the derivation of these operators we have made no assumptions about the grid structure . These operators are equally applicable to structured and unstructured grids.

6. DISCRETE FORM OF TENSOR ARTIFICIAL VISCOSITY

To complete the definition of the tensor viscosity an expression for the discrete viscosity coefficient is required.

For the discrete viscosity so satisfy the dissipativity condition μ must be non-negative, and constant for a corner. This second condition comes from the discrete expressions. Following the edge viscosity we base the tensor viscosity on the Kurapatenko form (5). So for a corner, μ is defined as

$$\mu_z^p = (1 - \psi_z^p)\rho_z^p \left\{ c_2 \frac{(\gamma+1)}{4} |\Delta \mathbf{v}_z^p| + \sqrt{c_2^2 \left(\frac{\gamma+1}{4}\right)^2 (\Delta \mathbf{v}_z^p)^2 + c_1^2 {c_{s,z}}^2} \right\} l_z^p. \quad (40)$$

$c_{s,z}$ is the speed of sound in zone z, c_1 and c_2 are non-dimensional, non-negative, constants. The corner density, ρ_z^p, is easily defined as the corner is a Lagrangian volume.

The viscosity coefficient requires the definition of a velocity jump, $\Delta \mathbf{v}_z^p$ and a characteristic length, l_z^p. The length is required to keep the dimensions of the viscosity tensor correct. The definition of these values have often caused difficulties in multi-dimensional shock viscosities [1]. Simple definitions of length, such as the square root of cell area in 2D, result in instabilities for large aspect ratio cells. Such cells do occur in practical problems. A more sophisticated approach is to calculate the shock direction in a cell, but this has proved difficult to do accurately and reliably. Again this approach has problems with large aspect ratio cells, where a small change in velocity or geometry can result in a large change in the length and velocity terms.

For the tensor viscosity we require definitions that do not cause problems for large aspect ratio cells, and are not sensitive to small changes in geometry. A simple definition of characteristic length for a corner volume is to use the length of the adjacent edge with direction closest to the shock direction. This choice did not result in a robust viscosity so an alternative was required. For the results presented in the next section the following length definition was used:

$$l_z^p = \begin{cases} 2 \times \sqrt{V_z^p} \sqrt{\frac{|\Delta \mathbf{x}_1|}{|\Delta \mathbf{x}_2|}} & \text{if } \widehat{\Delta \mathbf{x}}_1 \cdot \hat{\mathbf{v}}_{av} > \widehat{\Delta \mathbf{x}}_2 \cdot \hat{\mathbf{v}}_{av} \\ 2 \times \sqrt{V_z^p} \sqrt{\frac{|\Delta \mathbf{x}_2|}{|\Delta \mathbf{x}_1|}} & \text{if } \widehat{\Delta \mathbf{x}}_1 \cdot \hat{\mathbf{v}}_{av} \leq \widehat{\Delta \mathbf{x}}_2 \cdot \hat{\mathbf{v}}_{av}, \end{cases} \quad (41)$$

where

$$\mathbf{v}_{av} = 0.25(\mathbf{v}_p + \mathbf{v}_{p+\frac{1}{2}} + \mathbf{v}_z + \mathbf{v}_{p-\frac{1}{2}}). \quad (42)$$

Fig. 7 shows the definitions of the length and velocity terms used. The factor of 2 in the equation ensures that l_z^p is comparable in length to the adjacent edge. This definition gives a length that reflects the aspect ratio of the volume while being relatively insensitive to small changes in the velocity direction.

The velocity jump is taken as the maximum velocity jump across the corner volume

$$\Delta \mathbf{v}_z^p = 2 \times \max(|\Delta \mathbf{v}_1|, |\Delta \mathbf{v}_2|), \quad (43)$$

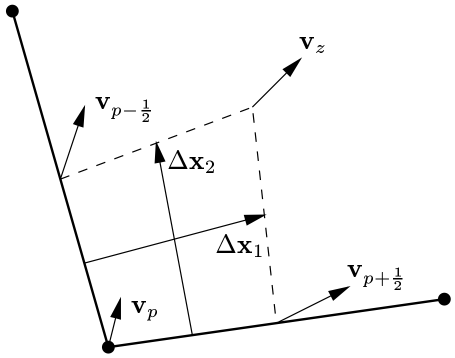

FIG. 7. Length and velocity definitions.

$\Delta\mathbf{v}_1$ and $\Delta\mathbf{v}_2$ are the velocity jumps along $\Delta\mathbf{x}_1$ and $\Delta\mathbf{x}_2$ respectively.

The final term to be defined is the limiter function ψ_z^p, which is calculated from the limiter values on the adjacent edges

$$\psi_z^p = \min(\psi_{p+\frac{1}{2}}, \psi_{p-\frac{1}{2}}). \tag{44}$$

For edge k the limiter function is

$$\psi_k = \min(\psi_1, \psi_2) \tag{45}$$

where

$$\begin{aligned} \psi_1 &= \max[0, \min(0.5(r_{l,k} + r_{r,k})\,,\, 2r_{l,k}\,,\, 2r_{r,k}\,,\, 1)] \\ \psi_2 &= \max[0, \min(0.5(r_{m,k} + r_{p,k})\,,\, 2r_{m,k}\,,\, 2r_{p,k}\,,\, 1)]. \end{aligned} \tag{46}$$

For edge k the r terms are

$$\begin{aligned} r_{l,k} &= \frac{(\mathbf{div}\ \mathbf{v})_l}{(\mathbf{div}\ \mathbf{v})_k} \quad , \quad r_{r,k} = \frac{(\mathbf{div}\ \mathbf{v})_r}{(\mathbf{div}\ \mathbf{v})_k} \\ r_{a,k} &= \frac{(\mathbf{div}\ \mathbf{v})_a}{(\mathbf{div}\ \mathbf{v})_k} \quad , \quad r_{b,k} = \frac{(\mathbf{div}\ \mathbf{v})_b}{(\mathbf{div}\ \mathbf{v})_k} \end{aligned} \tag{47}$$

In addition to the left and right edges, which are the same as used for the edge viscosity limiter function, above a and below b edges are required. Fig. 8 shows how these neighbor edges are defined. For an edge the divergence is calculated for the quadrilateral volume formed by the two end points and the centers of the two adjacent zones, Fig. 8. In one dimension this function reduces to the same function as the edge viscosity limiter

It is possible to define a similar function that calculates a limiter value directly for a corner volume, by using the velocity divergence calculated for corner volumes. This is not suitable because the velocity at three of the four vertices of a corner is interpolated. The limiter function will switch off the viscosity if all neighbor

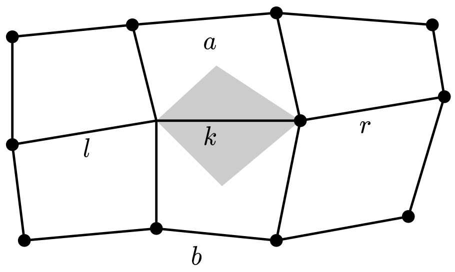

FIG. 8. Neighbor edges of edge k used for limiter function. The shaded area shows the volume used to calculate the divergence of velocity for the edge.

volumes have an equal or higher divergence. The effect of this is seen when the wave is aligned with the mesh, such as in a one dimensional calculation. In this case the divergence of velocity is constant for all corner volumes in a zone. This causes the viscosity to be switched off for corners on the upstream side of a zone when a shock wave passes through the zone.

It is convenient to calculate the viscosity force at a point in terms of corner forces, $\mathbf{f}_z^p$. A corner force is the force from zone z that acts on point p, so summing over the stencil of p gives the total force at the point. The discrete momentum equation at point p is written

$$m_p \frac{d\mathbf{v}_p}{dt} = V_p(\mathbf{DIV\ Q})_p = \mathbf{F}_p = \sum_{z\in S(p)} \mathbf{f}_z^p. \tag{48}$$

where m_p is the point mass. The viscosity corner force $\mathbf{f}_z^p$ is then

$$\begin{aligned}\mathbf{f}_z^p &= V_z\Bigg[\frac{1}{l_{p+\frac{1}{2}}}\left\{\frac{W_z^{p+1}}{\sin^2\theta_z^{p+1}}\left(\mu_z^{p+1}\mathbf{G}^e_{p+\frac{1}{2}} + \cos\theta_z^{p+1}\mu_z^{p+1}\mathbf{G}^e_{p+\frac{3}{2}}\right)\right\}\\ &+\frac{1}{l_{p+\frac{1}{2}}}\left\{\frac{W_z^{p}}{\sin^2\theta_z^{p}}\left(\mu_z^{p}\mathbf{G}^e_{p+\frac{1}{2}} + \cos\theta_z^{p}\mu_z^{p}\mathbf{G}^e_{p-\frac{1}{2}}\right)\right\}\\ &-\frac{1}{l_{p-\frac{1}{2}}}\left\{\frac{W_z^{p}}{\sin^2\theta_z^{p}}\left(\mu_z^{p}\mathbf{G}^e_{p-\frac{1}{2}} + \cos\theta_z^{p}\mu_z^{p}\mathbf{G}^e_{p+\frac{1}{2}}\right)\right\}\\ &-\frac{1}{l_{p-\frac{1}{2}}}\left\{\frac{W_z^{p-1}}{\sin^2\theta_z^{p-1}}\left(\mu_z^{p-1}\mathbf{G}^e_{p-\frac{1}{2}} + \cos\theta_z^{p-1}\mu_z^{p-1}\mathbf{G}^e_{p-\frac{3}{2}}\right)\right\}\Bigg]\end{aligned} \tag{49}$$

For zone z the discrete energy equation is

$$M_z \frac{de_z}{dt} = V_z(\mathbf{Q},\mathbf{G})_z\ . \tag{50}$$

Then using (38) it can be shown that the discrete energy equation becomes

$$M_z \frac{de_z}{dt} = -\sum_{p\in S(z)} \mathbf{f}_p^z \cdot \mathbf{v}_p\ . \tag{51}$$

These expressions are the discrete analogs of the continuous equations in section 3. So they retain the properties of the continuous equations, such as dissipativity.

Using the mimetic finite difference approach to derive these expressions ensures that total energy is conserved exactly, to numerical round off.

7. NUMERICAL RESULTS

The tensor artificial viscosity was implemented in a test code. The test code is a Lagrangian finite difference code which uses a compatible hydrodynamics algorithm [3]. The test code uses the Lagrangian subzonal pressure method to control grid distortion [4], and contains the edge viscosity developed by Caramana et al. [5] which is briefly described in section 2. Therefore we have one code which contains both the edge viscosity and the tensor viscosity, so when comparing results the only difference in the code used to produce them is the artificial viscosity.

As the viscosity has only been described in two dimensions, we only present test problems in two dimensional plane geometry. To avoid interaction of the subzonal pressures and the artificial viscosity obscuring differences in the viscosities, only a small subzonal pressure merit factor has been used. In all problems a merit factor of 0.1 was used, unless otherwise indicated.

We present results for three principal test problems which were used to investigate the behavior of the tensor viscosity. For all problems the coefficients c_1 and c_2 were both set to 1.0, for the tensor and edge viscosity.

7.1. Noh implosion problem

The Noh problem [12] is a well known test problem. Here the cylindrical implosion problem is used. A perfect gas with $\gamma = 5/3$ is given an initial unit inward radial velocity. A circular shock wave is generated at the center of convergence. At time 0.6 this shock wave has a radial coordinate of 0.2, and the density behind the shock is 16.0. Ahead of the shock the gas is compressed due to the convergence, and this produces a density profile with the equation $\rho = 1 + (t/R)$ where R is the radial coordinate and t the time.

Results are shown for an initially Cartesian mesh. The mesh is 50×50 zones, with the length of each edge is 1.0. Only a quarter of the volume is modeled, symmetry boundary conditions are used along the x and y axes. This problem is a test problem where then edge viscosity fails, Fig. 9. Along the axes jets form which result in a highly distorted mesh, subzonal pressures are required to allow the calculation to reach time 0.6. Increasing the merit factor just results in the jets becoming even more pronounced. The mesh can be improved by the c_1 viscosity coefficient to around 3.75 or higher, but this gives an error in the shock location and a very uneven density behind the shock, Fig. 10.

The tensor viscosity results show a circular shock of radius 0.2, and a smooth mesh behind the shock, Fig. 11. The density is not completely smooth behind the shock, with the zones on the line at 45° overestimating the density. This can be clearly seen in Fig. 12, which shows the density as a function of radius.

Results for both viscosities show the well known heating problem, which shows in the density profile as an underestimate near the point of convergence. We have not attempted to address this problem in the tensor viscosity as this is an inherent problem with shock physics codes [13], and solutions are available [6, 12].

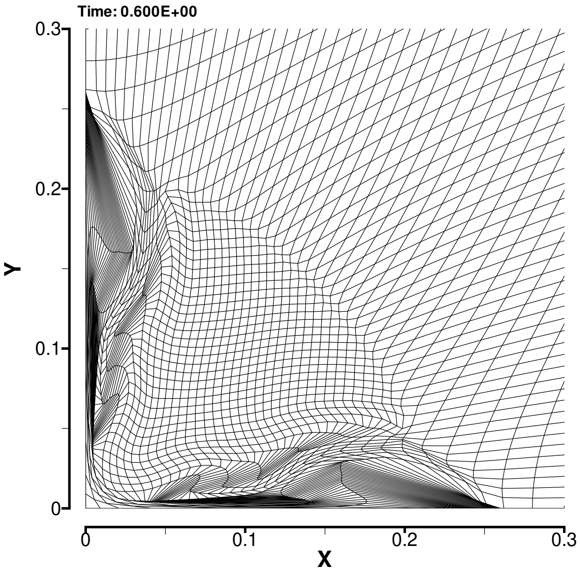

a

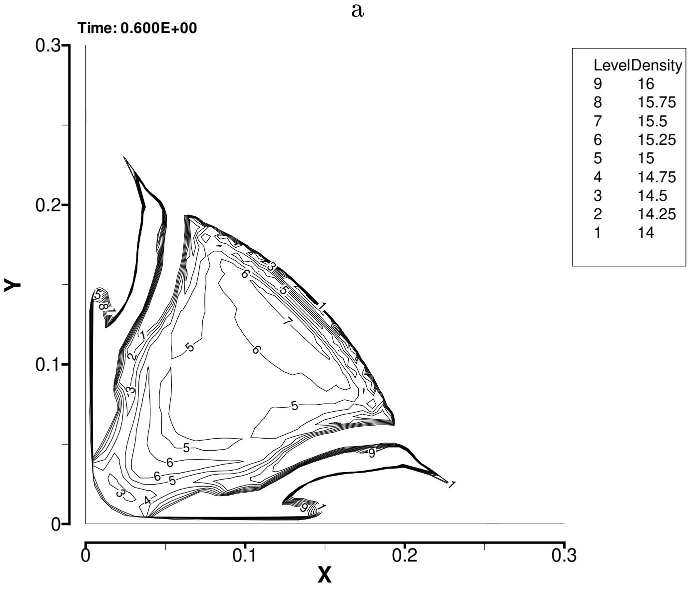

b

FIG. 9. Noh problem results on a Cartesian mesh for edge viscosity, merit factor = 0.1. (a) Mesh. (b) Density contour plot.

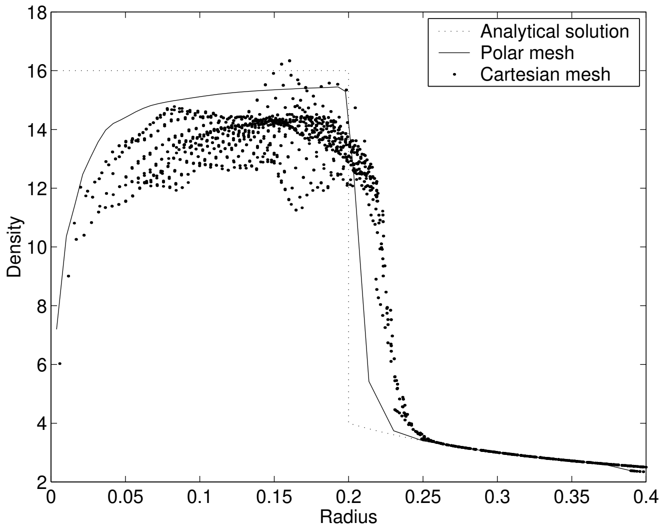

FIG. 10. Comparison of Noh problem results for polar ($c_1 = 1.0$) and Cartesian ($c_1 = 3.75$) grids for edge viscosity. For the Cartesian grid each point is a zone density plotted for the radius of the zone center.

7.2. Saltzman piston problem

In the Saltzman piston problem [11] a one dimensional shock wave propagates through a two dimensional mesh. This tests the ability of the code to model shock waves that are oblique to the mesh. As artificial viscosity is dominant in shock wave propagation, the Saltzman piston problem has often been used as in testing artificial viscosities [1, 2, 11].

The problem takes a box filled with gas, one end of the box is a movable piston. The piston moves into the box with a constant velocity of 1.0 and a strong shock wave is generated from the moving end. The gas is modeled using the ideal gas equation of state with $\gamma = 5/3$. The initial mesh is shown in Fig. 13. The initial length (x) is 1.0, and the height (y) is 0.1. The mesh is 100 zones in the x direction and 10 in the y direction. On the upper and lower boundaries symmetry boundary conditions are used. The nodal x coordinates are given as a function of their logical coordinates i, j by

$$x(i,j) = (i-1)dx + (11-j)\sin\left(\frac{\pi(i-1)}{100}\right)dy \tag{52}$$

where $dx = 1/100$ and $dy = 0.1/10$.

Results are shown for time 0.7 and time 0.925. At time 0.7 the shock has an x coordinate of 0.9333, and has not yet reached the fixed end. The density behind the shock is 4.0. By time 0.925, the shock has an x coordinate of 0.95, and is the third shock having reflected off the fixed and then moving ends. Now the density ahead of the shock is 10.0 and the density behind the shock is 20.0.

Both viscosities give good results for the Saltzman piston problem at time 0.7, Figs. 14–15. To reach time 0.925 using the edge viscosity subzonal pressures are required, otherwise the calculation stops shortly before time 0.925 due to grid dis-

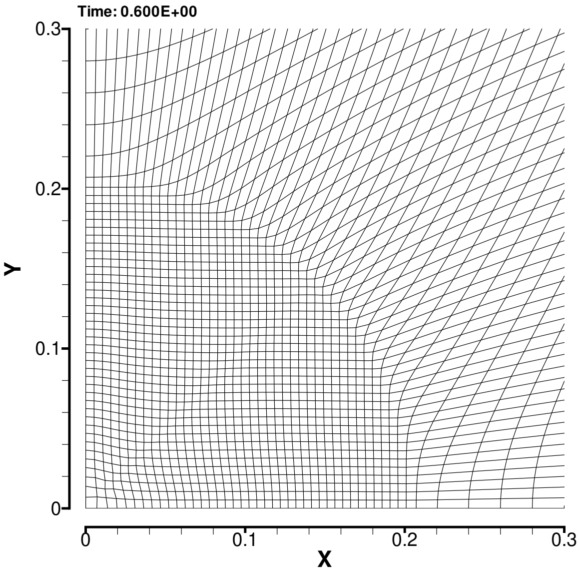

a

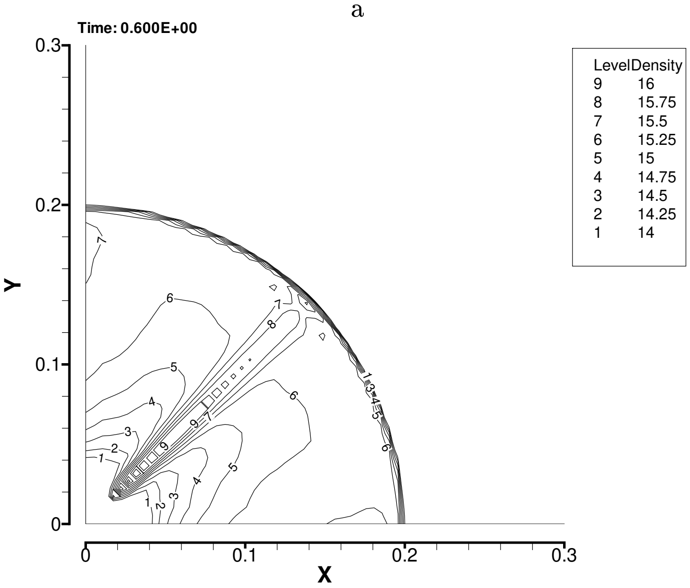

b

FIG. 11. Noh problem results on a Cartesian mesh for tensor viscosity, merit factor = 0.1. (a) Mesh. (b) Density contour plot.

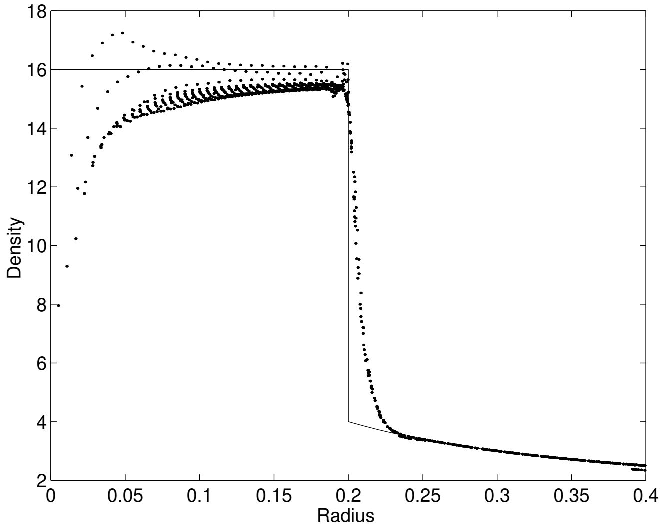

FIG. 12. Noh problem results for the tensor viscosity on a Cartesian grid, compared with the exact result. The zones with the high density all lie on a line at 45° to the coordinate axes.

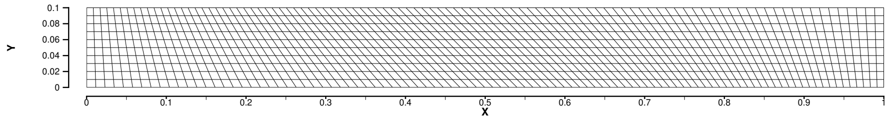

FIG. 13. Initial mesh for Saltzman piston problem. The piston moves from left to right at constant velocity.

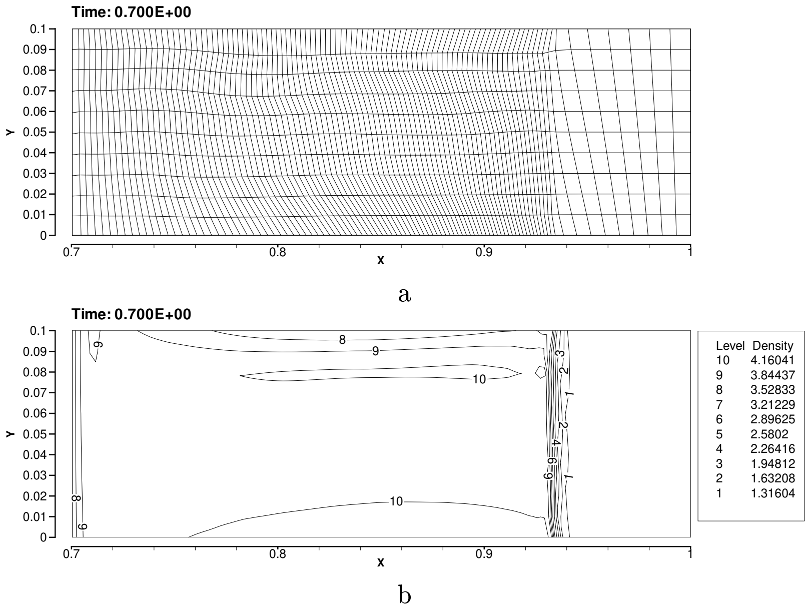

FIG. 14. Saltzman piston problem results for edge viscosity at t=0.7, merit factor = 0.1. (a) Mesh. (b) Density contour plot.

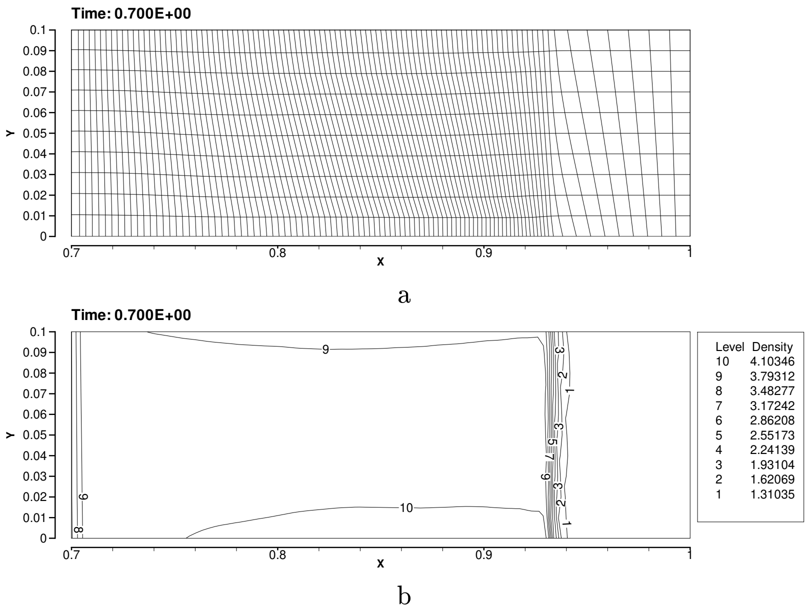

FIG. 15. Saltzman piston problem results for tensor viscosity at t=0.7, merit factor = 0.1. (a) Mesh. (b) Density contour plot.

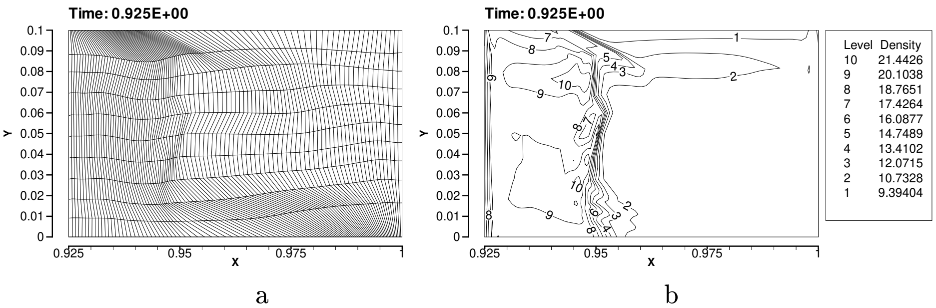

FIG. 16. Saltzman piston problem results for edge viscosity at t=0.925, merit factor = 0.1. (a) Mesh. (b) Density contour plot.

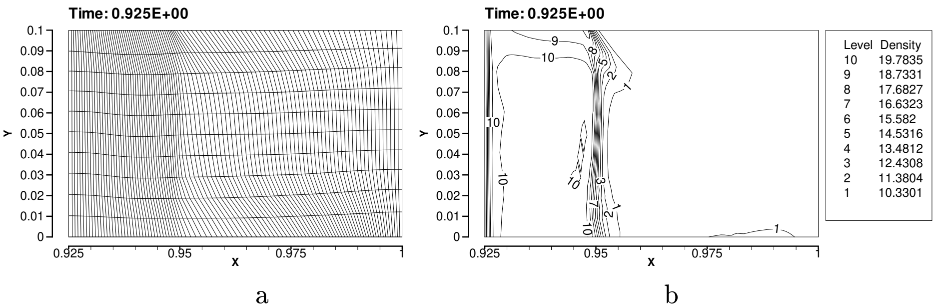

FIG. 17. Saltzman piston problem results for tensor viscosity at t=0.925, merit factor = 0.1. (a) Mesh. (b) Density contour plot.

tortion. The results for a merit factor of 0.1 show that the shock wave is no longer planar near the boundaries, Fig. 16. Increasing the merit factor produces a more even final mesh. The tensor viscosity results show a planar shock at time 0.925 with a merit factor of 0.1, Fig. 17. In his 1993 paper [2] Benson observes that for this problem it is generally true that a narrower shock results in a less uniform density behind the shock. Both viscosities give a similar shock front width of approximately 3–4 zones, so the shock width is not causing the variation in the smoothness of the density field.

7.3. Sedov blast wave problem

The Sedov blast wave problem [14] models the blast wave from an intense explosion in a perfect gas, so is an example of a diverging shock wave. The initial mesh is rectangular, consisting of 45×90 zones with a total edge length of 1.1 in both directions. The initial internal energy is zero except for the two zones closest to the origin, which have a specific internal energy of 409.7. These two zones form a square, so the initial conditions are symmetric about the 45° line. The analytic solution gives, for $\gamma = 1.4$, a shock of radius unity at time unity, and with a peak density of 6.0. The final solution should retain the symmetry about the 45° line of the initial conditions. As the initial mesh is rectangular and so not symmetric about this line, this problem provides a test of the ability of the code to maintain the symmetry of the problem when the computational grid does not embody this symmetry.

The edge viscosity now gives an elliptical shock front, with a larger radius along the x axis (45 zones) than the y axis (90 zones), Fig. 18. The tensor viscosity gives a smooth mesh but unlike the edge viscosity retains a circular shock, Fig. 19.

8. CONCLUSION

We have developed a multi-dimensional artificial viscosity that satisfies a set of conditions set out by Caramana et al. [5]. The viscosity is based on discrete approximations of the nonsymmetric velocity gradient tensor. Due to the tensor nature of the new viscosity, it reduces the dependence of the numerical solution on the grid. This is seen most clearly in results for the Noh problem on an initially square mesh, and the Sedov problem on an initially rectangular mesh. For both these problem the tensor viscosity retains the symmetry of the shock wave.

We have extended the mimetic discretization approach for general grids to tensor operators, deriving expressions for the gradient of a vector and divergence of a tensor. We have then used these discrete operators in the artificial viscosity. These operators can be used for any application where the gradient of a vector and divergence of a tensor are required.

Choosing to start from the gradient of velocity tensor means that the viscous force continuity condition has not been completely satisfied as there is no clear method of doing so.

The main area for future work is investigating different possibilities for viscosity coefficient and limiter function, as the test showed that these can have a strong effect on the results. This includes investigating forms of the coefficient that do fully satisfy the viscous force continuity condition.

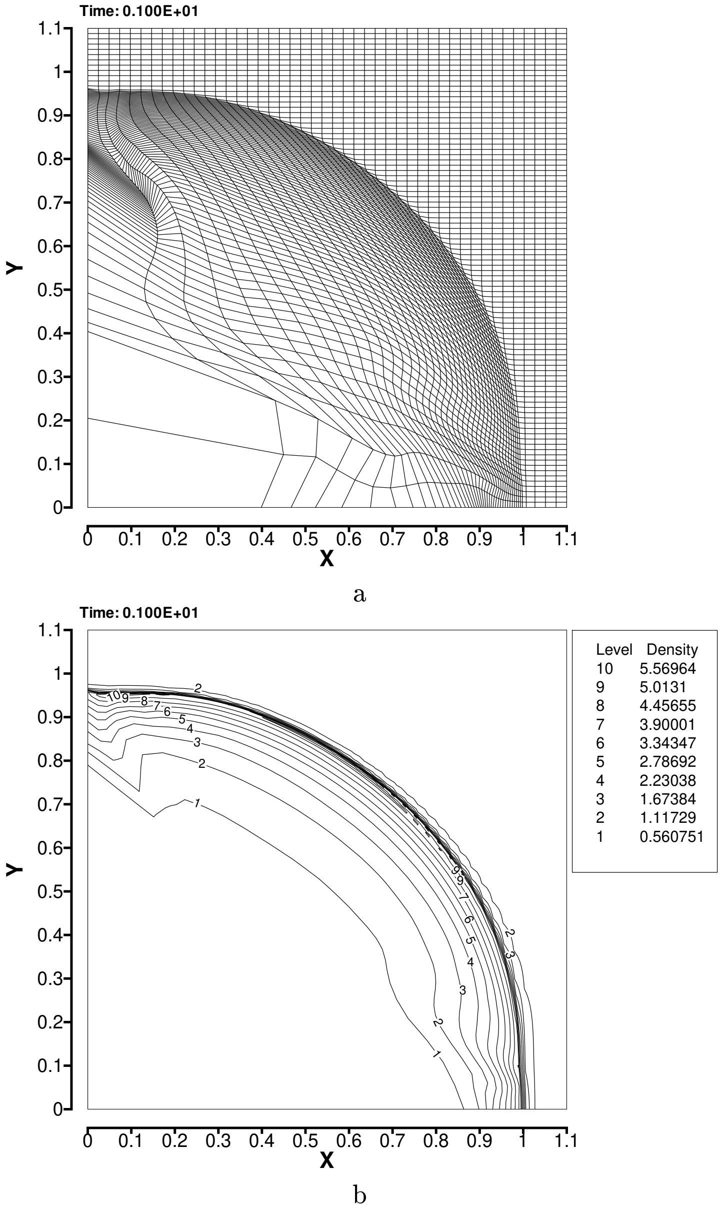

FIG. 18. 1:2 Sedov problem results for edge viscosity, merit factor = 0.1. (a) Mesh. (b) Density contour plot.

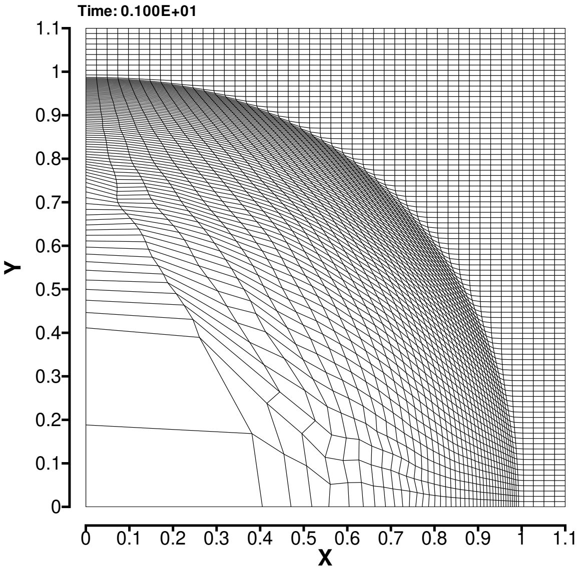

a

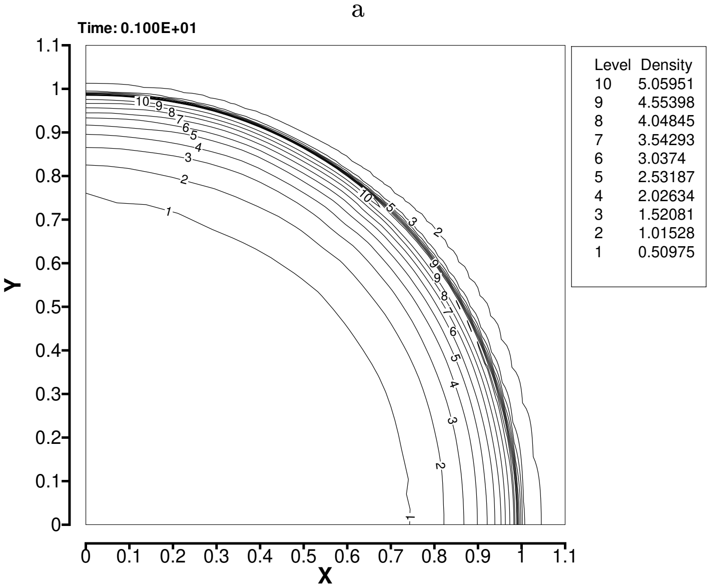

b

FIG. 19. 1:2 Sedov problem results for tensor viscosity, merit factor = 0.1. (a) Mesh. (b) Density contour plot.

ACKNOWLEDGMENT

We thank E. Caramana and L. Margolin for their useful comments and suggestions. This research was supported by the Department of Energy, under contract W-7405-ENG-36.

REFERENCES

1. D.J. Benson. A new two-dimensional flux-limited shock viscosity for impact calculations. *Computer Methods in Applied Mechanics and Engineering*, 93:39–95, 1991.
2. D.J. Benson and S. Schoenfeld. A total variation diminishing shock viscosity. *Computational Mechanics*, 11:107–121, 1993.
3. E.J. Caramana, D.E. Burton, M.J. Shashkov, and P.P. Whalen. The construction of compatible hydrodynamics algorithms utilizing conservation of total energy. *Journal of Computational Physics*, 146:227–262, 1998.
4. E.J. Caramana and M.J. Shashkov. Elimination of artificial grid distortion and hour-glass type motions by means of Lagrangian subzonal masses and pressures. *Journal of Computational Physics*, 142:521–561, 1998.
5. E.J. Caramana, M.J. Shashkov, and P.P. Whalen. Formulations of artificial viscosity for multi-dimensional shock wave computations. *Journal of Computational Physics*, 144:70–97, 1998.
6. R.P. Fedkiw, A. Marquina, and B. Merriman. An isobaric fix for the overheating problem in multimaterial compressible flows. *Journal of Computational Physics*, 148(545–578), 1999.
7. J.M. Hyman and M. Shashkov. Adjoint operators for the natural discretizations of the divergence, gradient and curl on logically rectangular grids. *Applied Numerical Mathematics*, 25:413–442, 1997.
8. J.M. Hyman and M. Shashkov. Natural discretizations for the divergence, gradient and curl on logically rectangular grids. *Computers & Mathematics with Applications*, 33(4):81–104, 1997.
9. V.F. Kurapatenko. *In: Difference methods for solutions of problems of mathematical physics, I (Editor: N.N. Janenko)*, page 116. Amer. Math. Soc., Providence, R.I., 1967.
10. R. Landshoff. A numerical method for treating fluid flow in the presence of shocks. Technical Report LA-1930, Los Alamos National Laboratory, 1955.
11. L.G. Margolin. A centered artificial viscosity for cells with large aspect ratios. Technical Report UCRL-53882, Lawrence Livermore National Laboratory, August 1988.
12. W.F. Noh. Errors for calculations of strong shocks using an artificial viscosity and an artificial heat flux. *Journal of Computational Physics*, 72:78–120, 1987.
13. W.J. Rider. Revisiting wall heating. *Journal of Computational Physics*, 162:395–410, 2000.
14. L.I. Sedov. *Similarity and dimensional methods in mechanics*. Academic Press, New York, 1959.
15. M. Shashkov and S. Steinberg. Solving diffusion equations with rough coefficients in rough grids. *Journal of Computational Physics*, 129:383–405, 1996.
16. J. Von Neumann and R.D. Richtmyer. A method for the calculation of hydrodynamic shocks. *Journal of Applied Physics*, 21:232–237, 1950.
17. M.L. Wilkins. Use of artificial viscosity in multidimensional fluid dynamic calculations. *Journal of Computational Physics*, 36:281–303, 1980.